

# Negative-index metamaterial at visible frequencies

Gunnar Dolling<sup>1,2</sup>, Martin Wegener<sup>1,2,3</sup>, Costas M. Soukoulis<sup>4,5</sup> & Stefan Linden<sup>2,3</sup>

<sup>1</sup>*Institut für Angewandte Physik, Universität Karlsruhe (TH), Wolfgang-Gaede-Straße 1, D-76131 Karlsruhe, Germany*

<sup>2</sup>*DFG-Center for Functional Nanostructures (CFN), Universität Karlsruhe (TH), D-76128 Karlsruhe, Germany*

<sup>3</sup>*Institut für Nanotechnologie, Forschungszentrum Karlsruhe in der Helmholtz-Gemeinschaft, D-76021 Karlsruhe, Germany*

<sup>4</sup>*Ames Laboratory and Department of Physics and Astronomy, Iowa State University, Ames, Iowa 50011, U.S.A*

<sup>5</sup>*Institute of Electronic Structure and Laser - Foundation of Research and Technology, Hellas, and Department of Materials Science and Technology, University of Crete, 71110 Heraklion, Crete, Greece*

**In 1951, G.D. Malyuzhinets<sup>1</sup> pointed out that a negative phase velocity  $c$  of an electromagnetic wave can be accomplished in certain periodic electronic circuits composed of capacitances  $C$  and inductances  $L$ . Here, “negative” refers to the backward direction opposite to the forward energy flow. If the resulting electromagnetic wavelength  $\lambda$  is larger than the circuit lattice constant  $a$ , the circuit can be considered as an effective medium with a negative index of refraction  $n$ . The miniaturization of the  $C$  and  $L$  components has led to 10 GHz operation frequency in 2001<sup>2</sup> and via intermediate steps<sup>3-9</sup> to frequencies around 200 THz<sup>10-13</sup> in the years 2005/2006, albeit with modified circuit designs<sup>14-16</sup>. In this letter, we fabricate a silver-based negative-index metamaterial at 384 THz visible frequency and give direct evidence for the negative phase velocity by phase-sensitive “time-of-flight” experiments.**

Photonic metamaterials are tailored artificial optical materials composed of sub-wavelength metallic building blocks that can be viewed as nano-scale electronic circuits. These building blocks or “atoms” are densely packed into an effective material such that the operation wavelength  $\lambda$  is ideally much larger than the lattice constant  $a$ . For a truly *effective* material, Bragg diffraction must not occur, i.e., at least the condition  $\lambda > 2a$  needs to be fulfilled. Along these lines, material properties become accessible that do not exist in natural substances, e.g., magnetism at optical frequencies<sup>5,7-9,17</sup>, a negative index of refraction<sup>10-13</sup>, cloaking of objects<sup>18,19</sup>, or frequency doubling mediated by the magnetic-field component of the light<sup>20</sup>. It is clear that increasing the operation frequency (equivalent to decreasing the wavelength  $\lambda$ ) requires miniaturization of both the “atoms” and the lattice constant. While the Maxwell equations are scalable, fundamental limits are

set by the metal plasma frequency. For operation frequencies even remotely approaching this limit, the resonance frequency approaches a constant<sup>21</sup> and Ohmic losses increase dramatically. Thus, it is not clear as to whether one can experimentally achieve today's "holy grail" of metamaterials, i.e., a negative index of refraction in the visible (375-750 THz frequency). At this point, one could literally "see" a highly nontrivial electronic circuit at work with the naked eye (Fig. 1a). While electronics and optics are usually considered to be two separate fields, they would merge into *one* here<sup>22</sup>.

The physics of the particular sample/circuit design used and miniaturized here has been described previously in work at lower frequencies<sup>10,12,13,16</sup>. In brief, for the polarization configuration shown in Fig. 1b, the metamaterial can be viewed as composed of two sets of sub-circuits or "atoms": (i) A coil with inductance  $L$  in series with two capacitors with net capacitance  $C$  as an  $LC$  circuit, providing a magnetic resonance at the  $LC$  resonance frequency<sup>14</sup>. (ii) Long metallic wires, acting like a diluted metal below the effective plasma frequency of the arrangement<sup>23</sup>. We use silver as constituent material because silver is known to introduce significantly lower losses<sup>24</sup> than, e.g., gold at visible frequencies. More than 50 samples with slightly different design parameters and with 100  $\mu\text{m}$  times 100  $\mu\text{m}$  footprint each, all on glass substrate coated with a 5-nm thin film of indium-tin-oxide (to avoid charging effects in the electron-beam-writing process), have been fabricated by us using standard electron-beam lithography, electron-beam evaporation of the constituent materials, and a lift-off procedure. Results obtained from the best sample of this set are presented in this letter. The electron micrograph of this sample shown in Fig. 1d reveals good large-scale homogeneity as well as 68-nm minimum lateral feature size at 97-nm thickness of the Ag-MgF<sub>2</sub>-Ag sandwich. This aspect ratio (i.e., height/width) exceeding unity poses significant fabrication challenges. Compared with our previous choice of parameters at lower frequencies<sup>12,13</sup>, especially the relative thickness of the metal wires oriented along the electric-field vector (i.e., the ratio  $w_y/a_y$  in Fig. 1c) had to be increased. This step increases the effective plasma frequency, which needs to be above the operation frequency in order to obtain a negative electric permittivity.

Figure 2a exhibits measured normal-incidence intensity transmittance and reflectance spectra of this metamaterial sample. The bare glass substrate and a silver mirror, respectively, serve as reference. Shown in Fig. 2b is the corresponding theoretical result based on numerical three-dimensional finite-difference time-domain calculations using the commercial software package *CST MicroWave Studio*. The geometrical parameters have already been indicated in Fig. 1c, optical material parameters taken are: MgF<sub>2</sub> refractive index  $n_{\text{MgF}_2}=1.38$ , glass substrate index  $n_{\text{substrate}}=1.5$ , and the Drude model for silver with plasma frequency  $\omega_{\text{pl}}=1.37\times 10^{16}$  / s and damping or collision frequency  $\omega_{\text{col}}=9\times 10^{13}$  / s. At the frequencies of interest here, the Drude model is an adequate description of the actual silver dielectric function<sup>24</sup>. The quoted damping has been chosen to match the experiment in the present work and especially comprises broadening effects due to any type of sample imperfection. The chosen damping is three times larger than the literature value<sup>24</sup>. Importantly, the exact same set of parameters will also be used below for the theoretical analysis of the interferometric experiments as well as for the effective-parameter retrieval.

An unambiguous determination of effective material parameters, especially of the phase velocity  $c=c_0/n$ , additionally requires phase-sensitive experiments. The details of the phase-sensitive “time-of-flight” experiment based on a compact and passively stable Michelson interferometer have been described previously by us<sup>12</sup>, albeit in a different wavelength regime. In essence, we record two interferograms, one with the metamaterial sample on its glass substrate in one of the interferometer arms, and a second interferogram with just the glass substrate by laterally moving the metamaterial out of the optical path. All mechanical motions are computer controlled and realized by precise and calibrated piezoelectric actuators. The corresponding shift on the interferometer time delay axis yields the phase delay due to the metamaterial. By tuning the center wavelength of the incident Gaussian transform-limited 125-fs pulses, derived from a commercial mode-locked Ti:Sa laser (*Spectra-Physics Tsunami*), and by repeating the described procedure for each wavelength, we measure phase-delay spectra. Simultaneously and similarly, we infer the shift between the two Gaussian interferogram envelopes at each wavelength, which provides us with the group-delay spectra. In essence, the group-delay spectrum is the spectral derivative of the phase-delay spectrum. Thus, the group-delay spectrum sensitively depends on the damping. Corresponding data (dots) are shown in Fig. 3a and Fig. 3b together with numerical calculations (solid curves), in which we derive the interferograms from the complex sample electric-field transmittance for the femtosecond pulse parameters as in the experiment and then proceed with the analysis as in the experiment. Finally, we retrieve<sup>25</sup> the effective material parameters from theory and depict them in Fig. 3c. These “retrieved” parameters refer to a fictitious homogeneous film on the glass substrate with a thickness identical to that of the metamaterial ( $d=97$  nm) and complex transmittance and reflectance properties strictly identical to those of the metamaterial on the glass substrate.

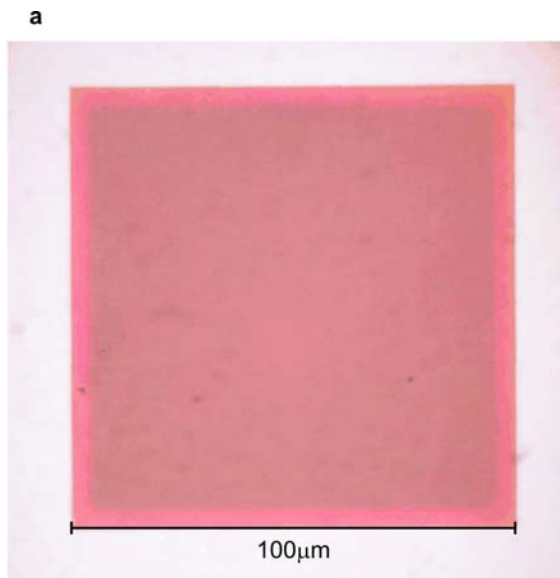
Obviously, the experimental results agree well with theory, which consistently describes transmittance, reflectance, phase-delay, as well as group-delay spectra – all with one set of parameters. Thus, the effective material parameters, especially the negative real part of  $n$  (Fig. 3c), retrieved from the same theory and the same parameters can be considered as very trustworthy. A determination on the basis of, e.g., intensity reflectance spectra alone would be ambiguous and not at all reliable based on our experience.

In conclusion, we have demonstrated a metamaterial with an effective real part of the index of refraction of -0.6 at around 780-nm wavelength. This goes beyond previous work in the visible<sup>17</sup> which showed a negative magnetic permeability. Phase-sensitive “time-of-flight” experiments give direct experimental evidence for the negative phase velocity of light, while the Poynting vector points into the forward direction. Studying the group velocity in parallel provides a sensitive consistency check of our analysis. As obvious from Fig. 3d, the figure of merit, FOM, defined via  $FOM=-\text{Re}(n)/\text{Im}(n)$ , is  $FOM=0.5$  at best, while best values of  $FOM=3$  have recently been achieved at 1400-nm wavelengths<sup>13</sup>. We believe that reducing and/or compensating the losses (via incorporating gain materials<sup>26</sup>) is the next crucial step for applications based on visible negative-index metamaterials.

We acknowledge support by the Deutsche Forschungsgemeinschaft (DFG) and the State of Baden-Württemberg through the DFG-Center for Functional Nanostructures (CFN) within subproject A1.5. The research of M. W. is further supported by project DFG-We 1497/9-1 and that of S. L. through a “Helmholtz-Hochschul-Nachwuchsgruppe” (VH-NG-232). The research of C. M. S. is further supported by the Alexander von Humboldt senior-scientist award 2002, by Ames Laboratory (Contract No. W-7405-Eng-82), EU projects PHOREMOST, METAMORPHOSE and DARPA (HR0011-05-C-0068).

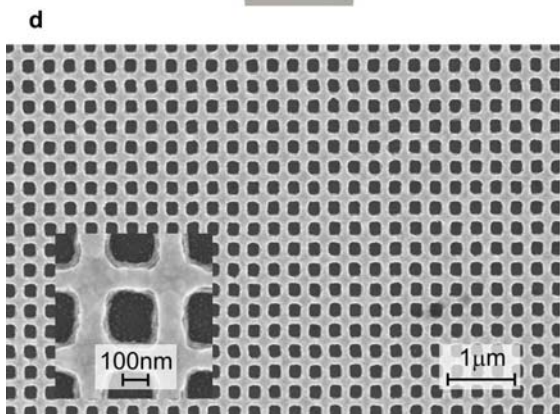
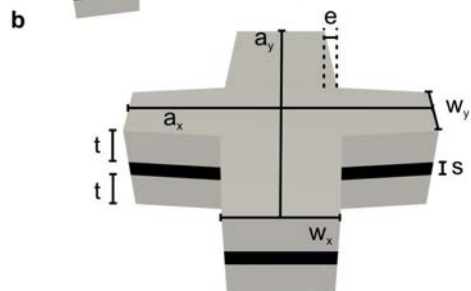
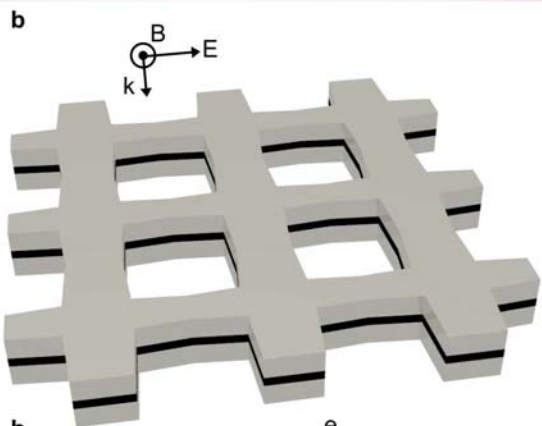
1. Malyuzhinets, G. D. A note on the radiation principle, *Zhurnal Technicheskoi Fiziki* **21**, 940-942 (1951).
2. Shelby, R. A., Smith, D. R. & Schultz, S. Experimental verification of a negative index of refraction, *Science* **292**, 77-79 (2001).
3. Yen, T. J. et al. Terahertz magnetic response from artificial materials, *Science* **303**, 1494-1496 (2004).
4. Smith, D. R., Pendry, J. B. & Wiltshire, M. C. K. Metamaterials and negative refractive index, *Science* **305**, 788-792 (2004).
5. Linden, S. et al. Magnetic response of metamaterials at 100 terahertz, *Science* **306** 1351-1353 (2004).
6. Katsarakis, N. et al. Magnetic response of split-ring resonators in the far-infrared frequency regime, *Opt. Lett.* **30**, 1348-1350 (2005).
7. Zhang, S. et al. Midinfrared resonant magnetic nanostructures exhibiting a negative permeability, *Phys. Rev. Lett* **94**, 037402 (2005).
8. Enkrich, C. et al. Magnetic metamaterials at telecommunication and visible frequencies, *Phys. Rev. Lett.* **95**, 203901 (2005).
9. Dolling, G. et al. Cut-wire pairs and plate pairs as magnetic atoms for optical metamaterials, *Opt. Lett.* **30**, 3198-3200 (2005).
10. Zhang, S. et al. Experimental demonstration of near-infrared negative-index metamaterials, *Phys. Rev. Lett.* **95**, 137404 (2005).
11. Shalaev, V. M. et al. Negative index of refraction in optical metamaterials, *Opt. Lett.* **30**, 3356-3358 (2005).
12. Dolling, G., Enkrich C., Wegener, M., Soukoulis, C. M. & Linden, S. Simultaneous negative phase and group velocity of light in a metamaterial, *Science* **312**, 892-894 (2006).
13. Dolling, G., Enkrich C., Wegener, M., Soukoulis, C. M. & Linden, S. Low-loss negative-index metamaterial at telecommunication wavelengths, *Opt. Lett.* **31**, 1800-1802 (2006).
14. Pendry, J. B., Holden, A. J., Robbins, D. J. & Stewart, W. J. Magnetism from conductors and enhanced nonlinear phenomena, *IEEE Trans. Microwave Theory Tech.* **47**, 2075 (1999).
15. Podolskiy, V. A. , Sarychev, A. K. , Narimanov, E. E. & Shalaev, V. M. Resonant light interaction with plasmonic nanowire systems, *J. Opt. A. Pure Appl. Opt.* **7**, 32 (2005).
16. Zhang, S. et al. Near-infrared double negative metamaterials, *Opt. Express* **13**, 4922-4930 (2005).

17. Grigorenko, A. N. et al. Nanofabricated media with negative permeability at visible frequencies, *Nature* **438**, 335-338 (2005).
18. Leonhardt, U. Optical conformal mapping, *Science* **312**, 1777-1780 (2006).
19. Pendry, J. B., Schurig, D. & Smith, D. R. Controlling electromagnetic fields, *Science* **312**, 1780-1782 (2006).
20. Klein, M. W., Enkrich, C., Wegener, M. & Linden, S. Second-harmonic generation from magnetic metamaterials, in press (2006).
21. Klein, M. W., Enkrich, C., Wegener, M., Soukoulis, C. M. & Linden, S. Single-slit split-ring resonators at optical frequencies: limits of size scaling, *Opt. Lett.* **31**, 1259-1231 (2006).
22. Engheta, N., Salandrino, A. & Alù, A. Circuit elements at optical frequencies: nanoinductors, nanocapacitors, and nanoresistors, *Phys. Rev. Lett.* **95**, 095504 (2005).
23. Pendry, J. B., Holden, A. J., Stewart, W. J. & Youngs, I. Extremely low frequency plasmons in metallic mesostructures, *Phys. Rev. Lett.* **76**, 4773 (1996).
24. Johnson, P. B. & Christy, R. W. Optical constants of the noble metals, *Phys. Rev. B* **6**, 4370 (1972).
25. Smith, D. R., Schultz S., P., Markoš, P. & Soukoulis, C. M. Determination of effective permittivity and permeability of metamaterials from reflection and transmission coefficients, *Phys. Rev. B* **65**, 195104 (2002).
26. Chettiar, U. K. et al., From low-loss to lossless optical negative-index materials, CLEO/QELS-06 Annual Meeting Proceedings, Long Beach, CA, May 21-26.



**Figure 1**

**a**, transmission-mode micrograph of the sample illuminated by white light, polarized as in **b**. **b**, scheme of the metamaterial and polarization configuration. **c**, unit cell of the structure with definition of parameters: lattice constant  $a_x=a_y=300$  nm,  $w_x=102$  nm,  $w_y=68$  nm,  $t=40$  nm,  $s=17$  nm, “error”  $e_x=e_y=e=8$  nm. **d**, top-view electron micrograph of the sample employed in Figs. 2 and 3. The inset shows a magnified view.



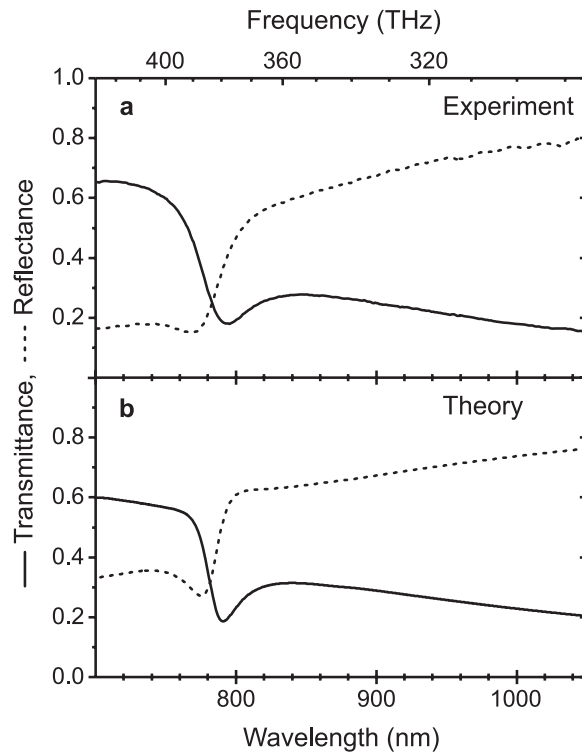


**Figure 2**

**a**, Measured transmittance (solid) and reflectance (dashed) spectrum of the negative-index metamaterial described in Fig. 1 for the polarization configuration of Fig. 1b. **b**, corresponding theoretical calculation. The exact same parameters are used in the calculations depicted in Fig. 3.

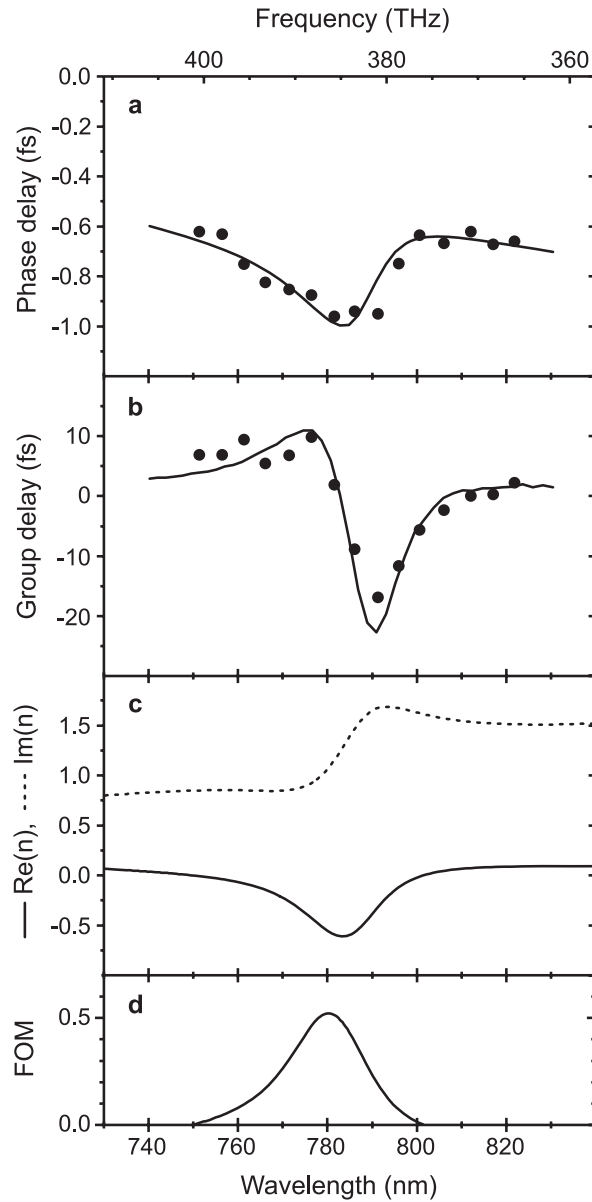


**Figure 3**

**a**, Measured (dots) phase delay versus laser center wavelength for a pulse propagating through the metamaterial sample characterized in Figs. 1 and 2 and for the polarization configuration depicted in Fig. 1b. The solid curve is the corresponding theoretical calculation. **b**, group delay versus wavelength. **c**, retrieved real (solid) and imaginary (dashed) part of the effective refractive index  $n$ . **d**, resulting figure of merit  $\text{FOM} = -\text{Re}(n) / \text{Im}(n)$ . The identical set of sample parameters is used in all calculations shown in Figs. 2 and 3.